Journal of Chemical&Engineering Data

pubs.acs.org/jced

Article

Thermodynamic Inhibition of CO_2−CH_4 Gas Hydrates by DESs: Experimental and Computational Study

Njabulo Mziwandile Zulu,* Hamed Hashemi, Kaniki Tumba, and Victoria T. Adeleke

Cite This: *J. Chem. Eng. Data* 2025, 70, 3675−3689

Read Online

ABSTRACT: This study presents an experimental and computational investigation of thermodynamic hydrate inhibition behavior of four deep eutectic solvents (DESs) on binary mixed CO_2−CH_4 gas hydrates. The mixtures of hydrogen bond acceptors, tetramethylammonium chloride, and tetrapropylammonium bromide with hydrogen bond donors, glycerol, and ethylene glycol were used to prepare the DESs. The hydrate liquid−vapor equilibrium data for studied systems were measured using an isochoric pressure-search method within the temperature and pressure ranges of (280.51−285.20) K and (3.86−9.48) MPa, respectively. All the investigated DESs inhibited CO_2−CH_4 hydrates, with the inhibition effect increasing with the DES concentration. The experimental results were validated using a computational approach through the analysis of sigma profile data and hydrogen bonding energies obtained for the investigated DESs. The order of the obtained sigma profile results and hydrogen bonding energies was consistent with the experimental results, thereby validating the inhibition ability of the investigated DESs. The hydrogen bonding energies that were obtained in this study correlated well with the inhibition ability of the studied DESs, and this proved the reliability of the computational approach used. Furthermore, this computational approach was successfully used as the prescreening tool to predict the inhibition ability of theoretically formulated DESs without experimental data.

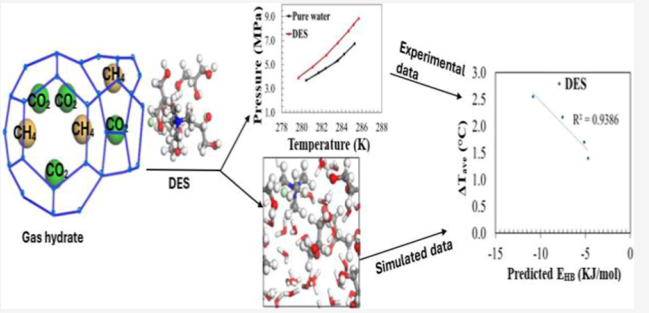

INTRODUCTION

Gas hydrates are ice-like crystalline compounds that are formed in the presence of water and gas molecules under high pressure and low temperature conditions.[1] The gas molecules (guests) are encapsulated in cavities (host) that are made of hydrogen-bonded water molecules.[1] The formation of gas hydrates in the oil and gas industry has a negative impact on flow assurance because it may result in the blockages of transmission lines, thereby interrupting operations. Therefore, it is in the interest of the oil and gas industry to urgently seek cost-effective and environmentally friendly measures to prevent gas hydrate formation.

Various mitigation methods have been proposed to prevent the formation of gas hydrates, and these include dehydration, thermal heating, depressurization, and chemical inhibition.[2] Among these gas hydrate mitigation methods, chemical inhibition is the most used approach.[2,3] Chemical inhibition involves the addition of chemical compounds to keep the gas flowlines outside the gas hydrate formation conditions.[2] These compounds, which are known as chemical inhibitors, either alter the gas hydrate phase behavior or delay the formation of the gas hydrate. There are two major types of chemical inhibitors, namely, thermodynamic hydrate inhibitors (THIs) and low dosage hydrate inhibitors (LDHIs). THIs shift the hydrate equilibrium curve toward lower temperature and higher-pressure regions, while LDHIs delay the formation of the gas hydrate.[3,4]

The selection of these chemical inhibitors is based on the economic, safety, and environmental aspects.[1,5,6] Although the currently used THIs have been found to be effective,[3] their application is limited due to high cost and negative environmental impact related to their use.[1] Notwithstanding that LDHIs require lower injection rates than THIs,[3] their poor performance at high pressure, high subcooling, and high-water cuts conditions upholds THIs as the robust choice for effective inhibition of gas hydrates.[7] A constant search for cost-effective and environmentally friendly THIs remains a matter of interest for many researchers. It is evident from research associated with gas hydrate inhibition that substances that have strong electrostatic charges and also form hydrogen bonding with water are effective THIs.[8]

Received: February 7, 2025
Revised: May 14, 2025
Accepted: August 6, 2025
Published: August 15, 2025

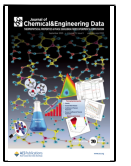

Green solvents known as deep eutectic solvents (DESs) have been discovered as cost-effective and environmentally friendly solvents that could be a sound alternative to the currently used THIs because they have functional groups that are capable of forming hydrogen bonds with water.[9,10] Besides exhibiting negligible vapor pressure, DESs have high biodegradability and low toxicity.[11,12] DESs are commonly prepared from two or more salts as the hydrogen bond acceptors (HBAs) and hydrogen bond donors (HBDs).[10,13] Generally, the resulting solvent has a melting point lower than those of both HBA and HBD.[14]

DESs have been proposed by various researchers as potential green solvents for mitigating flow assurance problems associated with gas hydrate formation in the oil and gas industry.[10] The inhibition mechanism of three deep eutectic solvents as potential shale inhibitors in water-based drilling fluids was investigated by Jia et al.[15] The potential of choline and urea-based DESs as thermodynamic hydrate inhibitors of methane gas hydrates was demonstrated by Lee et al.[16] Tetraethylammonium acetate and tetraethylammonium bromide-based DESs were identified as thermodynamic inhibitors for carbon dioxide hydrate formation by Sivabalan et al.[17] In the investigation by Khoo et al.,[18] reline DES acted as both kinetic and thermodynamic inhibitors of methane gas hydrates. Furthermore, Rasool et al.[19] found in their study that the addition of choline chloride and urea-based DES inhibited the formation of methane gas hydrates.

It is evident from these few studies that the phase equilibrium data related to the gas hydrate-forming systems in the presence of DESs are limited. This is likely to hinder the investigation of the inhibition effect of DESs on gas hydrate formation. Hence, more work is still required to validate DESs as gas hydrate inhibitors. It is worth noting that there is also a lack of computational studies in this respect, especially on mixed CO_2−CH_4 hydrate systems. This study is aimed at investigating the effectiveness of a selected variety of deep eutectic solvents in preventing the formation of mixed carbon dioxide and methane gas hydrates. Once their effectiveness is established, they could be introduced into industrial applications to address the current gap of cost-effective and environmentally friendly inhibitors.

In the present study, the effects of tetramethylammonium chloride and tetrapropylammonium bromide-based DESs on the equilibrium conditions of mixed carbon dioxide and methane clathrate hydrates are investigated. There are four DESs that are synthesized and characterized from a combination of glycerol and ethylene glycol (EG) as the HBDs and tetramethylammonium chloride (TMAC) and tetrapropylammonium bromide (TPAB) as the HBAs. The combinations of HBAs/HBDs were formed at a 1:3 molar ratio, respectively. Both experimental and computational approaches are used in this study. The experimental hydrate phase equilibrium conditions of the systems containing the mixture of CO_2 and CH_4 + DES + water are reported within the temperature and pressure ranges of (280.51−285.20) K and (3.86−9.48) MPa, respectively. The concentrations of DES in the aqueous solutions are 0.02 and 0.04 mass fractions. The performance of the studied DESs is evaluated by measuring the extent of shifting the phase equilibrium curve to higher pressure and lower temperature regions.

Furthermore, the experimental approach for measuring the thermodynamic data is costly and time-consuming, and hence an appropriate computational approach to predict and validate the inhibition effect of DESs should also be used. A widely used predictive tool is the conductor-like screening model for real solvents (COSMO-RS) model, which estimates interactions between water and inhibitor molecules by analyzing the electron charge distribution of each substance, such as the sigma (σ)-profile.[20,21] The sigma profile is suitable for molecular evaluation of potential gas hydrate inhibitors, and it is therefore presented in this study to validate the thermodynamic inhibition behavior of all studied DESs.

Additionally, the hydrogen bonding energy has been reported to be closely related to the inhibition ability of materials that form hydrogen bonds with water.[22,23] Hence, the inhibition effects of the investigated DESs are further validated through the determination of the hydrogen bonding energy between water and DES molecules. This hydrogen bonding energy was calculated using the supermolecular method suggested by Gordon and Jensen.[24]

Lastly, the prediction of gas hydrate inhibition ability in the absence of experimental data was carried out using sigma profile analysis and hydrogen bonding strengths for the combinations of DESs that were not tested in this study. Through this approach, the scope of DESs awaiting experimental investigation can be narrowed down by prescreening ineffective gas hydrate inhibitors.

EXPERIMENTAL AND COMPUTATIONAL METHODS

Experimental Section. *Materials.* Materials used for this study are outlined in Table 1, and they include distilled water,

Table 1. Supplier, Purity, and CAS Registry Number of Chemicals Used[a]

chemical	supplier	purity (mass fraction)[a]	CAS no.
tetrapropylammonium bromide	Sigma-Aldrich	≥0.980	1941−30−6
tetramethylammonium chloride	Sigma-Aldrich	≥0.980	75−57−0
ethylene glycol	Sigma-Aldrich	≥0.990	107−21−1
glycerol	Sigma-Aldrich	≥0.995	56−81−5
CO_2−CH_4 mixture	Afrox-SA	0.500[b]	
water	lab-purified	≥0.999	7732−18−5

[a]No additional purification was done; water content for TPAB, TMAC, EG, and glycerol was 3.8×10^{-4}, 3.9×10^{-4}, 4.2×10^{-4}, and 4.5×10^{-4}, respectively. [b]Mole fraction.

50−50 mol % CO_2−CH_4 gas mixture, and DESs. Distilled water was obtained from the research laboratory at Mangosuthu University of Technology (MUT), where this work was conducted. All the gases were supplied by AFROX (South Africa). All the DES components were supplied by SIGMA-Aldrich. The chemical structures of DES constituents are shown in Table 2.

Experimental Apparatus and Procedure. *Preparation and Characterization of DESs.* The DESs were prepared and characterized, and their typical compositions are listed in Table 3. An accurate analytical balance, model AS220/C/2 (supplied by RADWAG, Poland) with an uncertainty of $\pm 1 \times 10^{-7}$ kg in mass, was used to prepare DESs having an uncertainty level of $\pm 5 \times 10^{-7}$ m^3 gravimetrically.

The preparation and purification of DESs were carried out using the procedure described by several researchers in the literature.[25−27] The investigated DESs were prepared by

https://doi.org/10.1021/acs.jced.5c00067
J. Chem. Eng. Data 2025, 70, 3675−3689

Table 2. Chemical Structures of the DES Constituents Used in This Work

Chemical Name	Chemical Structure
Hydrogen Bond Acceptors	
Tetramethylammonium Chloride	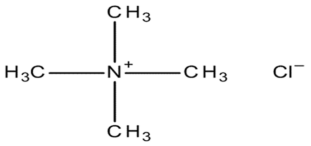
Tetrapropylammonium Bromide	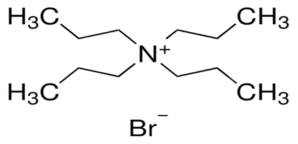
Tetramethylammonium Hydroxide	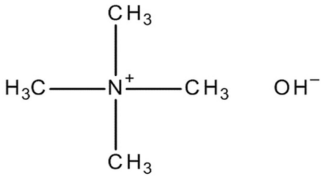
Tetraethylammonium Chloride	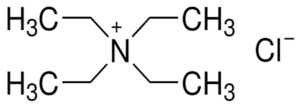
Hydrogen Bond Donors	
Glycerol	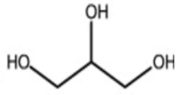
Ethylene Glycol	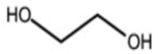
Urea	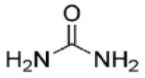

Table 3. Compositions and Abbreviations for the Studied DESs

molar ratio	abbreviation
1 TPAB: 3 glycerol	DES 1
1 TPAB: 3 EG	DES 2
1 TMAC: 3 glycerol	DES 3
1 TMAC: 3 EG	DES 4

mixing the hydrogen bond acceptor (HBA) with the hydrogen bond donor (HBD) according to the desired HBA-to-HBD molar ratio. The two components were thoroughly mixed at a specified temperature using a magnetic stirrer until a clear homogeneous liquid was obtained. The prepared DES was purified by subjecting it to a temperature of 373.15 K in an oven for 8 h to remove traces of impurities and moisture. The obtained solution was stored in an airtight container to prevent exposure to moisture.

Characterization of each DES that had been prepared was carried out using density, viscosity, and refractive index (RI) measurements. Density and refractive index were measured according to the methods outlined in the literature.[28−30] The refractive index and density were measured using an Atago refractometer (model RX-7000) and an Anton Paar density and sound velocity meter (model DSA 500M), respectively. Prior to DES property measurements, calibration of both pieces of equipment was undertaken by measuring the refractive index and density of ultrapure water at a specified temperature.

Measurements of viscosity were carried out according to the method described by Mbatha et al.[31] The viscosity of DES was measured using an Anton Paar AMVn rolling-ball viscometer. Prior to the experimental analysis, ethanol was used to clean the cell, and acetone was used for drying using the automatic Xsample 452 module. Prior to the viscosity measurements, the water calibration was done at 298.15 K to ensure that the equipment would produce valid results. An uncertainty of 0.004 was obtained.

Apparatus. A schematic diagram of the experimental apparatus, which was used in this study, is shown in Figure 1. This experimental setup is similar to that which was used by Nkosi et al.[32] The main part of the apparatus is a high-pressure equilibrium cell made of stainless steel (SS 316L) material (supplied by Büchi, Switzerland) with an internal volume of 100 mL. The interior of the cell was hydrophobically coated with an alloy (nickel−chromium-iron−molybdenum), which was capable of withstanding temperatures and pressures up to 473.15 K and 10 MPa, respectively. A four-wire Pt-100 thermocouple (supplied by Grant Instruments, United Kingdom), with an uncertainty of ±0.3 K, was fitted within the cell to monitor the temperature of the system. A pressure transducer (supplied by ESI Technology, United Kingdom) having an uncertainty of ±0.25% of full scale was used to measure the inside pressure of the cell. A magnetic stirrer with a capacity of 1000 rpm was installed to ensure proper mixing of the contents of the cell. A temperature-controlled unit named LTC4 (supplied by Grant Instruments, United Kingdom) consisting of a TX150 Optima circulating bath and an R4 tank/refrigeration unit was used. It allowed setting and controlling the system temperature, corresponding to the liquid bath temperature. The coolant was an aqueous solution of glycerol water. Any trapped air inside the cell was removed by a vacuum pump (supplied by Gardner Denver, United States). The apparatus was connected to an SQ2020-1F8 data acquisition unit (supplied by Grant Instruments, United Kingdom) and interfaced with a computer to monitor pressure and temperature data at intervals using SquirrelView software.

Procedure. The dissociation conditions for this study were measured using the isochoric pressure-search method (graphical technique), as described by Sloan and Koh[1] and Tumba et al.[6] The equilibrium cell was evacuated before being fed with the aqueous solution and the gas.

After initial evacuation, the appropriate quantity of the aqueous solution (approximately 40 cm^3 with an uncertainty level of ±0.5 cm^3) was injected into the equilibrium cell, which was then immersed in the temperature-controlled bath. The

https://doi.org/10.1021/acs.jced.5c00067
J. Chem. Eng. Data 2025, 70, 3675−3689

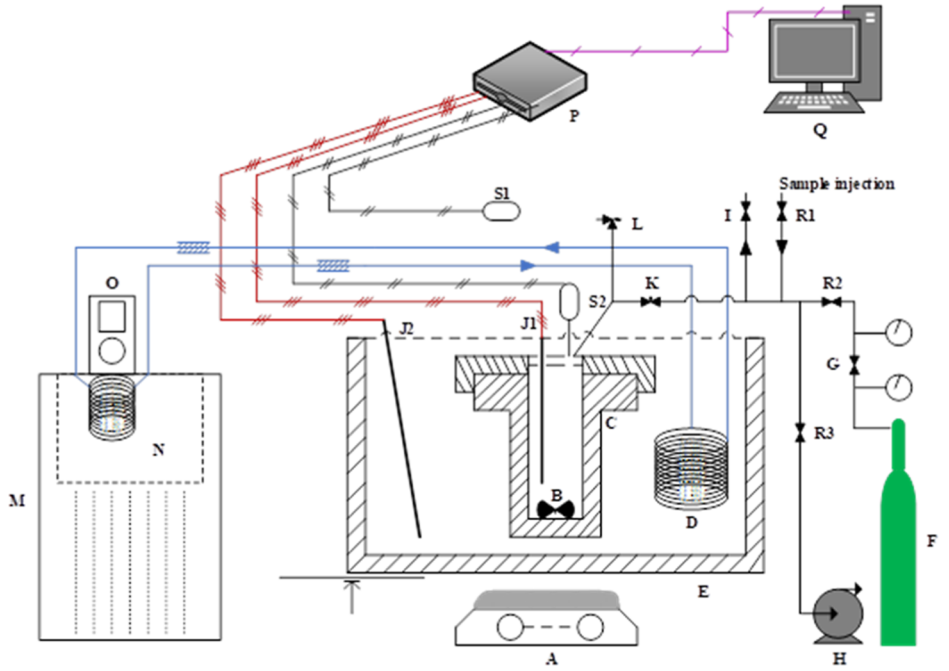

Figure 1. Schematic diagram for the high-pressure equilibrium apparatus: (A) magnetic stirrer; (B) neodymium magnet stir bar; (C) high-pressure equilibrium cell; (D) cooling coil; (E) thermostated bath; (F) gas cylinder; (G) pressure regulator; (H) vacuum pump; (I) vent valve; (J1 and 2) temperature probes (Pt-100); (K) needle valve for loading; (L) relief valve; (M) LTC4 unit; (N) LTC4 unit built-in circulating bath; (O) circulating thermostat; (P) data acquisition system; (Q) computer; (R1−3) shut-off valve; and (S1 and 2) pressure transducers reproduced from ref 32. Copyright [2022] American Chemical Society.

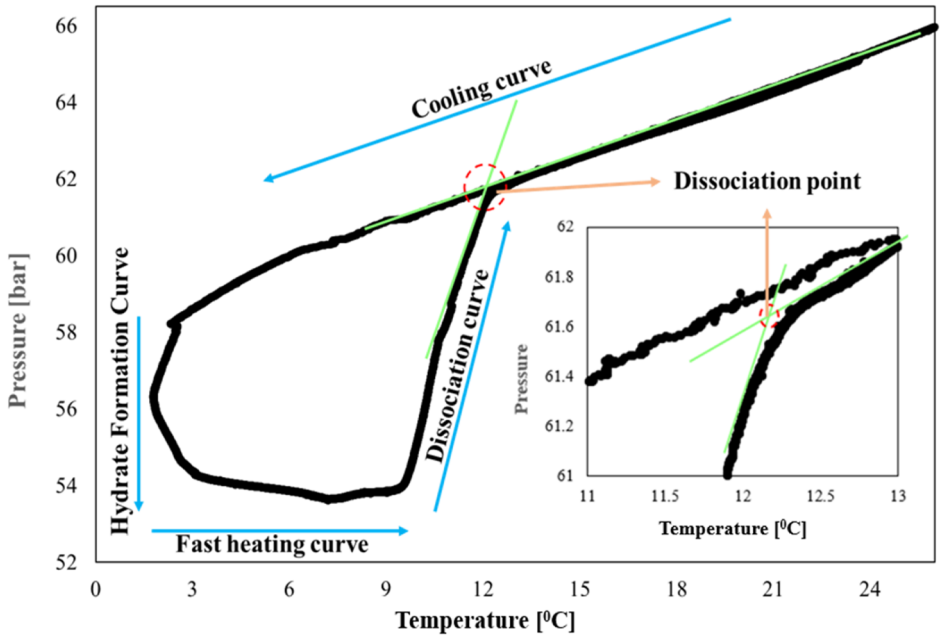

Figure 2. Pressure versus temperature trace for the formation and dissociation of gas hydrate.

gas was then supplied into the cell from a gas cylinder through a pressure regulation valve for gas hydrate formation. After obtaining the stability of temperature and pressure, the valve for the gas line was closed. The system temperature was slowly reduced from the vapor−liquid region, which resulted in a slight decrease in pressure. A certain temperature was reached at which the hydrate was formed, and this was detected by a remarkable drop in pressure. After the formation of the hydrate, the temperature was slowly increased in steps of 0.1 K to initiate the dissociation process, and this resulted in a quick rise in pressure. At every temperature step, the temperature was kept constant for a sufficient time to achieve the state of equilibrium within the cell.

For each experimental run, a pressure versus temperature diagram was drawn, from which the hydrate dissociation point was obtained. The hydrate dissociation point was the point where the hydrate dissociation trace intersected with the initial cooling trace, as shown in Figure 2.

https://doi.org/10.1021/acs.jced.5c00067
J. Chem. Eng. Data 2025, 70, 3675−3689

Table 4. Chemical Compounds and Models

chemical	formula	CAS no.	models
water	H_2O	7732−18−5	DFT/DMol3/GGA-PBE/DNP/COSMO-RS
tetrapropylammonium bromide	$C_{12}H_{28}BrN$	1941−30−6	
tetramethylammonium chloride	$C_4H_{12}ClN$	75−57−0	
tetramethylammonium hydroxide	$C_4H_{13}NO$	75−59−2	
tetraethylammonium chloride	$C_8H_{20}ClN$	56−34−8	DFT/CASTEP/GGA-PBE
ethylene glycol	$C_2H_6O_2$	107−21−1	
glycerol	$C_3H_8O_3$	56−81−5	
Urea	CH_4N_2O	57−13−6	

Table 5. Density (ρ) of Tested DESs at T = (293.15−323.15 K) and Atmospheric Pressure[a]

DES	ρ/g cm^{-3}						
	293.15 K	298.15 K	303.15 K	308.15 K	313.15 K	318.15 K	323.15 K
DES 1	1.2094	1.2064	1.2034	1.2003	1.1973	1.1943	1.1913
DES 2	1.1393	1.1366	1.1335	1.1302	1.1266	1.1227	1.1185
DES 3	1.1692	1.1661	1.1631	1.1594	1.1563	1.1524	1.1497
DES 4	1.0621	1.0596	1.0571	1.0546	1.0522	1.0498	1.0475

[a]Standard uncertainties are u(T) = 0.05 K, u(P) = 0.1 kPa, u(ρ) = 2 × 10^{-3} g·cm^{-3}.

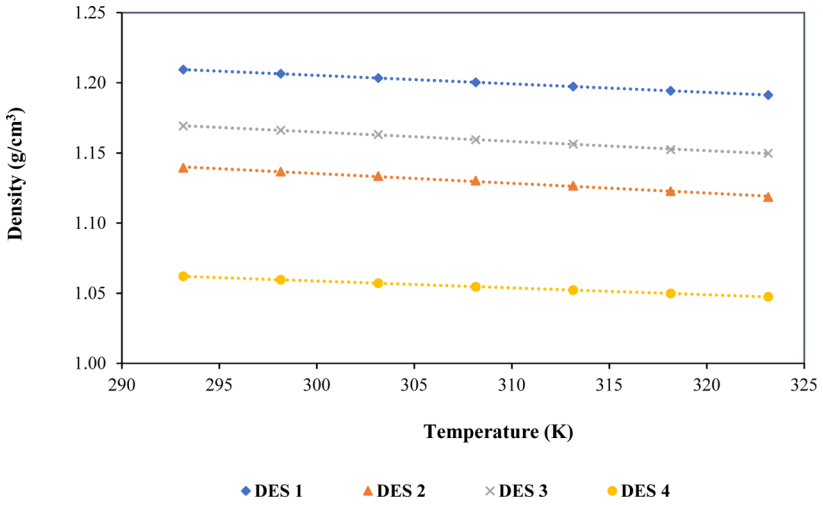

Figure 3. Variation of density with temperature for different DESs at T = (293.15−323.15 K).

Average Suppression Temperature Calculation. The average suppression temperatures (ΔT_{ave}) of the DESs were calculated to determine the thermodynamic inhibition effects of the studied deep eutectic solvents. The inhibition effect is following equation[33]

$$\Delta T_{ave} = \frac{\sum \Delta T}{n} = \frac{\sum_{i=0}^{n} (T_0 - T)}{n} \quad (1)$$

where ΔT is defined as the difference between the hydrate dissociation temperature in the absence (T_0) and presence (T) of DESs. The n denotes the number of hydrate dissociation points considered. The values of both dissociation temperatures were obtained from the same dissociation pressure.

Quantum Chemical Analysis. Chemical compounds and models used in the computational section of this study are outlined in Table 4.

COSMO-RS Analysis of the DES−Water System. A detailed description of the COSMO-RS model is found elsewhere in the literature.[20,21] Thus, only the concept relevant to gas hydrate inhibition is presented. Molecular interaction through sigma profiles of DESs and water molecules is generated using the COSMO-RS model to determine the gas hydrate inhibition ability of DESs. The generation of sigma profiles is carried out in two basic steps. First, the structure of DES is built and optimized with Material Studio 2020 software using DMol3 module with parameters set as generalized gradient approximation of the Perdew−Burke−Ernzerhof (GGA-PBE) level of density functional theory (DFT) along with the double numerical plus polarization (DNP) basis set. Second, the sigma profiles are generated using the COSMO-RS model by selecting water and the optimized structure of DES.

Hydrogen Bonding Energy Prediction. Reliable and consistent information on the stability of different types of hydrogen-bonded complexes comes from the density functional theory (DFT) calculations. DFT has established itself as a universal tool for electronic structure calculations.[34] The intermolecular interaction energy is directly estimated as the energy lost by complexation of molecules using quantum chemical calculations known as the supermolecular approach. This was carried out in two steps. First, the structures of DES, water, and DES−water complex were built and optimized

https://doi.org/10.1021/acs.jced.5c00067
J. Chem. Eng. Data 2025, 70, 3675−3689

Table 6. Viscosity (μ) of Tested DESs at T = (293.15−323.15 K) and Atmospheric Pressure

DES	mPa.s						
	293.15 K	298.15 K	303.15 K	308.15 K	313.15 K	318.15 K	323.15 K
DES 1	910.18	712.05	544.47	407.43	300.94	225.00	179.60
DES 2	88.31	73.08	59.75	48.33	38.83	31.23	25.54
DES 3	535.97	374.94	268.77	196.94	146.83	112.35	88.81
DES 4	37.39	30.56	24.50	19.21	14.71	10.97	8.01

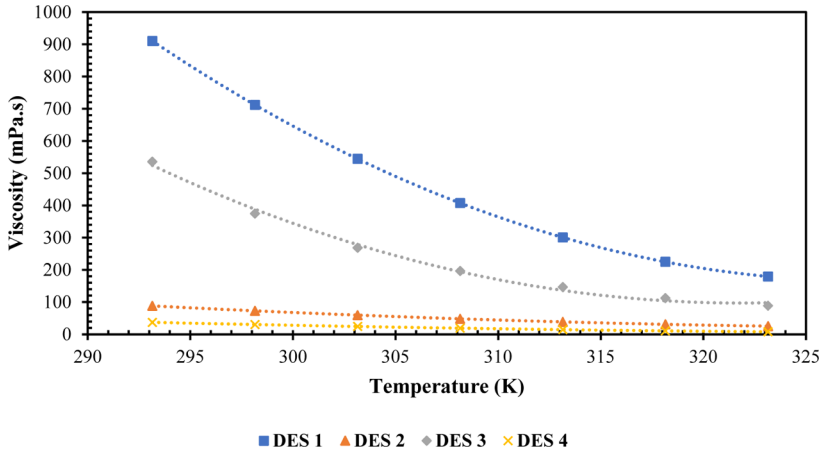

Figure 4. Variation of viscosity with temperature for different DESs at T = (293.15−323.15 K).

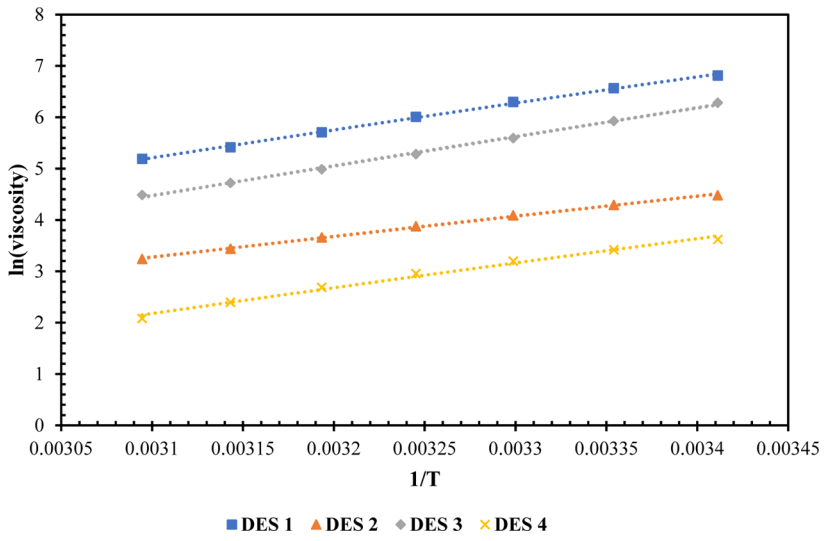

Figure 5. Plot of ln (viscosity) vs 1/T.

using the CASTEP tool in Material Studio. The exchange−correlation functions were GGA-PBE with the convergence tolerance energy of 2×10^{-5} eV/atom, maximum force of 5×10^{-2} eV/Å, maximum stress of 0.1 GPa, and maximum displacement of 2×10^{-3} Å. The electronic minimization parameters were set with an energy cutoff of 489.80 eV, SCF tolerance of 2×10^{-6} eV/atom, maximum SCF cycles of 100, Pulay in the density mixing scheme, and density mixing charge of 0.5−1.5 $Å^{-1}$.

In this approach, the energy of interaction between DES and water (W) molecules in the DES−water complex can be calculated as follows

$$\Delta E = E(\mathrm{DES} + \mathrm{W})_{\mathrm{complex}} - E(\mathrm{DES}) - E(\mathrm{W}) \quad (2)$$

where E denotes the electronic energies of the respective species.[24] ΔE must be corrected to account for basis set superposition errors (BSSE). A counterpoise (CP) method that was proposed by Boys and Bernadi is used to overcome the superposition by ensuring the simultaneous optimization of geometries of dimeric complexes along with their components according to the following equation[35]

$$\mathrm{BSSE} = E[\mathrm{DES}] + E[\mathrm{W}] - E[\mathrm{DES(W)}] - E[\mathrm{W(DES)}] \quad (3)$$

where E[DES] is the energy of fragment DES with its basis function, while E[DES(W)] is the energy of the same fragment DES in the presence of the basis function on water.

$$\Delta E^{\mathrm{CPC}} = \Delta E + \mathrm{BSSE} \quad (4)$$

https://doi.org/10.1021/acs.jced.5c00067
J. Chem. Eng. Data 2025, 70, 3675−3689

Table 7. Refractive Index (RI) of Tested DESs at T = (293.15−323.15 K) and Atmospheric Pressure[b]

DES	RI						
	293.15 K	298.15 K	303.15 K	308.15 K	313.15 K	318.15 K	323.15 K
DES 1	1.4886	1.4877	1.4866	1.4854	1.4842	1.4828	1.4814
DES 2	1.4767	1.4756	1.4744	1.4730	1.4717	1.4702	1.4686
DES 3	1.4669	1.4659	1.4649	1.4638	1.4625	1.4612	1.4598
DES 4	1.4545	1.4536	1.4525	1.4514	1.4502	1.4488	1.4474

[b]Standard uncertainties are u(T) = 0.05 K, u(P) = 0.1 kPa, u(RI) = 1.2 × 10^{-3}.

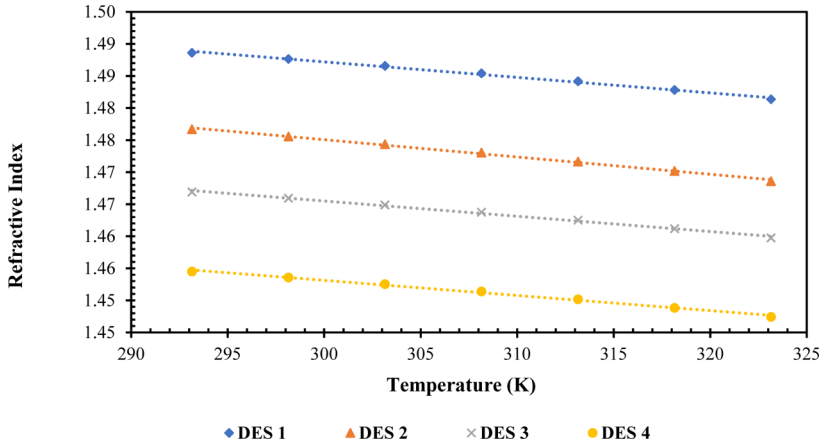

Figure 6. Variation of RI with temperature for different DESs at T = (293.15−323.15 K).

The hydrogen bond energy was calculated by dividing the ΔE^{CPC} by the number of water molecules involved.

RESULTS AND DISCUSSION

Characterization of DESs. The density measurements of DESs at a temperature range of 298.15−323.15 K are presented in Table 5 and Figure 3. The density values obtained varied from 1.0475 to 1,2094 g/cm^{3,} depending on temperature and HBA/HBD combination. The ethylene glycol-based DESs presented values ranging from 1.0475 to 1.1393 g/cm^{3,} while the glycerol-based DESs had values that range from 1.1497 to 1.2094 g/cm^3. The density values for all DESs decreased with the increase in temperature. This is illuminated by the increase in the free space between the pure components of DES, resulting from higher thermal agitation, which causes a decrease in the amount of bulk solvent molecules.[36] As shown in Table 8, the regression analysis of density for all DESs displays a linear relationship (R^2 > 0.994) between density and temperature, which is consistent with literature reports for other DES systems.[37]

The viscosity measurements of DESs investigated in this study are presented in Table 6 and Figure 4. The viscosity values obtained varied from 8.01 to 910.18 mPa.s depending on temperature and HBA: HBD combination. The ethylene glycol-based DESs presented values ranging from 8.01 to 88.31 mPa.s, while the glycerol-based DESs had values ranging from 88.81 to 910.18 mPa.s. It is observed that the DES viscosity decreases with an increase in temperature. This is related to the substantial decrease in hydrogen bonding interaction as the temperature rises, which causes an increase in the mobility of DES components.[36] Figure 5 shows the plotting of ln (viscosity) versus 1/T, which was the basis of the regression analysis for viscosity as a function of temperature. As presented in Table 8, the regression analysis of viscosity for all DESs shows a linear relationship (R^2 > 0.991) between viscosity and temperature, which is consistent with literature reports for other DES systems.[38]

The refractive index measurements of DESs investigated in this study are presented in Table 7 and Figure 6. The studied DESs had RIs ranging from 1.4474 to 1.4886, depending on temperature and HBA/HBD combination. Glycerol-based DESs had higher RIs than the equivalent EG-based DESs. This is aligned with the RIs of pure components, whereby glycerol has a value of 1.4746, which is higher than 1.4318 for EG. Like the observation for density and viscosity, the RIs decreased with an increase in temperature. This reduction in RI results from the decrease in density, which improves the mobility of light. As shown in Table 8, the regression analysis of RI for all DESs demonstrates a linear relationship (R^2 > 0.995) between RI and temperature, which is consistent with literature reports for other DES systems.[39]

Table 8. Regression Analysis of Density (ρ), Viscosity (μ), and Refractive Index Versus Temperature Data for Tested DESs over the Temperature Range (293.15−323.15 K)

DES	R^2		
	density	viscosity	refractive index
DES 1	1.0000	0.9984	0.9952
DES 2	0.9948	0.9989	0.9968
DES 3	0.9987	0.9972	0.9953
DES 4	0.9998	0.9915	0.9952

Hydrate-Liquid−Vapor (H-L−V) Equilibrium Data. Table 9 and Figures 7 and 8 summarize the equilibrium conditions obtained for 50−50 mol % carbon dioxide-methane mixture clathrate hydrates at 2 and 4 wt % concentrations of DES in aqueous solution. The reliability of the experimental method is demonstrated by the reasonable agreement between the experimental data for carbon dioxide−methane mixture

https://doi.org/10.1021/acs.jced.5c00067
J. Chem. Eng. Data 2025, 70, 3675−3689

Table 9. Hydrate (or H-L-V) Phase Equilibrium Data of the CH_4 + CO_2 Mixture (50/50 Mol %) in Water with and without 2 wt % and 4 wt % Aqueous DES Solutions[a]

water		DES1		DES2		DES3		DES4	
T(K)	P(MPa)	T(K)	P(MPa)	T(K)	P(MPa)	T(K)	P(MPa)	T(K)	P(MPa)
CH4 + CO2+ 2 wt % DES + water									
280.80	3.86	280.73	4.12	280.89	4.04	280.85	4.35	280.66	4.29
281.68	4.31	281.31	4.51	281.95	4.69	281.63	4.96	281.96	5.16
282.40	4.69	282.23	5.10	282.65	5.15	282.89	5.93	282.80	5.77
283.60	5.46	283.23	5.82	283.60	5.77	283.74	6.62	283.67	6.41
284.24	5.87	284.04	6.43	284.19	6.19	284.51	7.35	284.49	7.17
285.15	6.63	284.98	7.31	284.99	6.77	285.10	7.99	285.05	7.69
CH4 + CO2+ 4 wt % DES + water									
280.80	3.86	280.85	4.67	280.51	4.26	280.58	5.03	280.88	4.99
281.68	4.31	281.70	5.27	281.39	4.82	281.14	5.44	281.39	5.39
282.40	4.69	282.46	5.81	282.73	5.80	282.42	6.59	282.37	6.16
283.60	5.46	283.62	6.83	283.54	6.51	283.65	7.75	283.52	7.26
284.24	5.87	284.67	7.82	284.55	7.40	284.70	8.92	284.43	8.30
285.15	6.63	285.19	8.36	285.06	7.85	285.20	9.48	285.18	9.16

[a]Standard uncertainty: $u(T)$ (0.95 level of confidence) = ± 0.08 K, $u(P)$ (0.95 level of confidence) = ± 0.0234 MPa K and u(DES molar ratio) = 0.005.

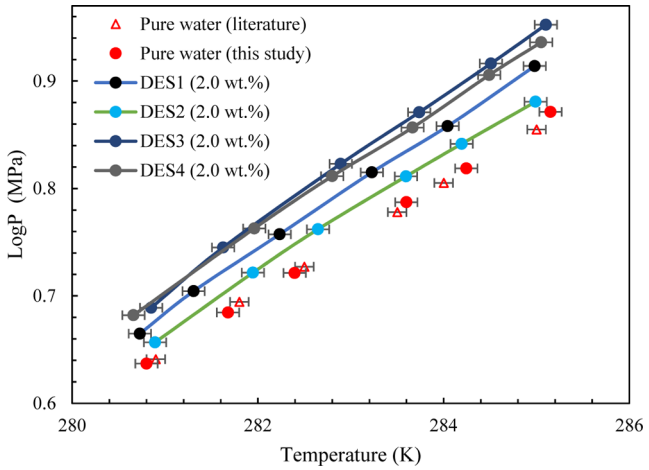

Figure 7. Thermodynamic stability condition curves for the clathrate hydrate of the CH_4 + CO_2 + H_2O system with and without DES inclusion (2.0 wt %).

hydrates in pure water from this study and those reported in the literature.[40] All the four studied DESs have demonstrated thermodynamic inhibition effects on mixed carbon dioxide and methane clathrate hydrates by shifting of hydrate dissociation conditions to higher pressure and lower temperature regions in comparison to that of the pure water system. The order of the equilibrium boundary shift arranged from the maximum to the minimum is DES 3 > DES 4 > DES 1 > DES 2. From the pattern observed, it is evident that for HBAs, tetramethylammonium chloride is superior to tetrapropylammonium bromide, while glycerol is superior to ethylene glycol for HBDs. This thermodynamic inhibition effect is dependent on the concentration of DES in the aqueous solution as higher inhibition ability is observed at 4 wt % concentration in comparison to that of 2 wt %.

Average Suppression Temperatures (ΔT_{ave}). The average suppression temperatures (ΔT_{ave}) were also calculated for 2 and 4 wt % DES solutions for a further comparison of the impact demonstrated by the studied DESs on mixed carbon dioxide-methane hydrate equilibrium temperature. The obtained results are presented in Table 10 and graphically plotted in Figure 9.

The results also proved that DES 3 demonstrated superior thermodynamic gas hydrate inhibition ability as compared to the rest of the investigated DESs. The degree of suppression achieved by DES 3 is 1.35 K at 2 wt % and 2.55 K at 4 wt %, whereas for the lowest achiever, DES 2, it is 0.46 K at 2 wt % and 1.40 K at 4 wt %. Similarly, the suppression behavior arranged from the highest to the lowest is DES 3 > DES 4 > DES 1 > DES 2. This suppression behavior is achieved due to the hydrogen bonding of cations and anions part of DESs with water molecules.[41]

Table 11 shows the average suppression temperatures of commercial thermodynamic inhibitors (methanol and ethylene glycol) calculated from the phase equilibrium data that were obtained from literature.[42] For comparative analysis, Figure 10 represents the average suppression temperatures at 4 wt % of the studied systems with the commercial thermodynamic inhibitors at 10 wt %. According to the results shown, the inhibition performance of commercial THIs is unsurpassed; however, the behavior of DES 3 and DES 4, which are closer to ethylene glycol with the value of 2.82 K, displayed that DESs have great potential to be effective green thermodynamic hydrate inhibitors. Although the performance of commercial THIs has not been exceeded, various combinations of DESs in future studies would give comparable results in light of similar concentration levels. This would be possible due to the synergistic effect of DES components, which would arise because of the combination of two inhibitors that produce an inhibition effect that is greater than the sum of their individual behavior.

Validation Section. *Sigma Profile Interpretation.* A sigma profile graph in COSMO-RS allows us to understand certain aspects of a DES−water system. The main information that is obtained from the graph is to learn about the hydrophobicity of DES and the hydrogen bond donor or hydrogen bond acceptor part of DES. The sigma profile graph is divided into three sections, which include the hydrogen bond donor region (at the left of −0.01 e/A^2), the nonpolar region (between −0.01 and 0.01 e/A^2), and the acceptor region (at the right of 0.01 e/A^2). The tendency of the DES part to act as a hydrogen

https://doi.org/10.1021/acs.jced.5c00067
J. Chem. Eng. Data 2025, 70, 3675−3689

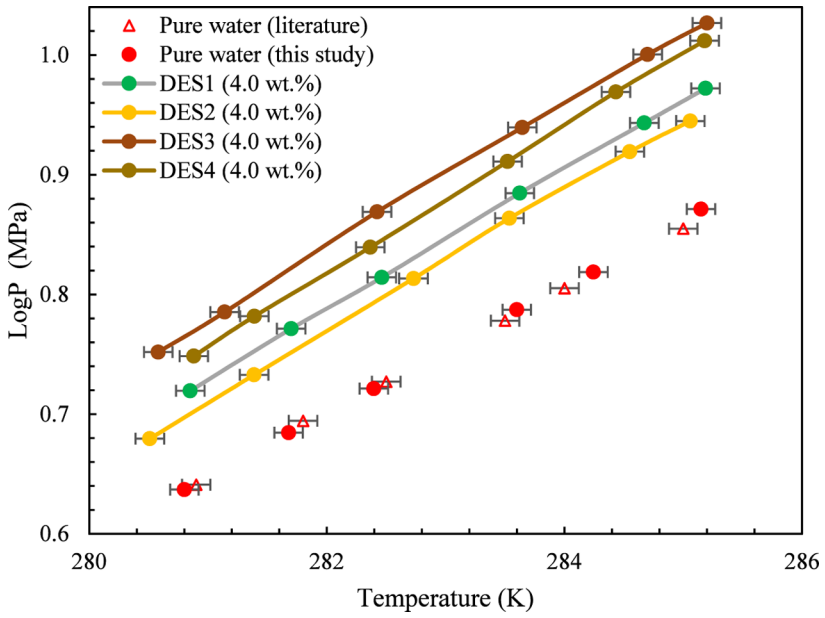

Figure 8. Thermodynamic stability condition curves for the clathrate hydrate of the CH_4 + CO_2 + H_2O system with and without DESs inclusion (4.0 wt %).

Table 10. Average Suppression Temperature Data for the CH_4+ CO_2 (50/50 mol %) Gas Mixture System

	DES 1		DES 2		DES 3		DES 4	
	2 wt %	4 wt %	2 wt %	4 wt %	2 wt %	4 wt %	2 wt %	4 wt %
P(MPa)	$\Delta T(K)$		$\Delta T(K)$		$\Delta T(K)$		$\Delta T(K)$	
4.5	0.75	1.46	0.41	1.15	1.00	2.20	1.06	1.79
5.0	0.91	1.66	0.58	1.36	1.30	2.46	1.27	2.10
5.5	1.02	1.78	0.62	1.50	1.48	2.60	1.39	2.28
6.0	0.93	1.73	0.48	1.44	1.42	2.63	1.29	2.23
6.5	0.88	1.76	0.38	1.47	1.41	2.65	1.23	2.27
7.0	0.95	1.80	0.30	1.50	1.46	2.75	1.29	2.35
$\Delta T_{ave}(K)$	0.91	1.70	0.46	1.40	1.35	2.55	1.26	2.17

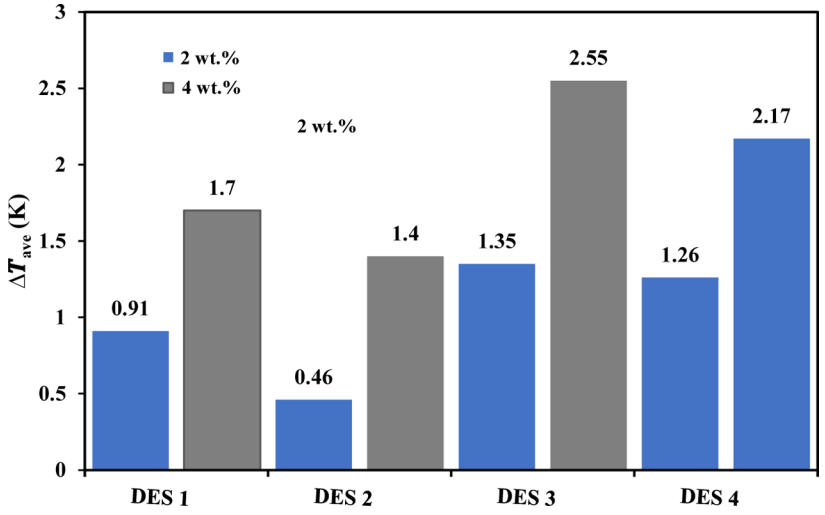

Figure 9. Average temperatures of the studied DESs for the CH_4 + CO_2 + H_2O system.

bond donor or acceptor would be identified by the location of the peak of that part on the graph. The sigma profile displays the affinity of DES toward water molecules, although it does not directly calculate a value that represents the gas hydrate inhibition ability of DES. The hydrophilicity of DES increases with its affinity toward water molecules, and this results in an increased DES−water interaction. This will then increase the effectiveness of DES as a gas hydrate inhibitor. Hence, in this section, two sigma profile graphs are used to determine the affinity of each DES toward the water molecules.

https://doi.org/10.1021/acs.jced.5c00067
J. Chem. Eng. Data 2025, 70, 3675−3689

Table 11. Average Suppression Temperature Data of Commercial Thermodynamic Inhibitors (Methanol and Ethylene Glycol) for the Mixed CH_4-CO_2 Gas System

	methanol	ethylene glycol
	10 wt % (5.88 mol %)	10 wt % (3.12 mol %)
P(MPa)	$\Delta T(K)$	$\Delta T(K)$
4.5	5.04	2.84
5.0	5.12	2.89
5.5	5.06	2.81
6.0	5.07	2.80
6.5	5.10	2.80
7.0	5.13	2.80
$\Delta T_{ave}(K)$	5.09	2.82

Hydrogen Bond Acceptor Part. *Anion Effect.* Figure 11 shows the sigma profile graph of TMAC, TPAB, and water molecules. It is observed that water has two high peaks, one in the hydrogen bond donor region and another in the acceptor region, and this indicates that water has a high affinity toward both acceptor and donor.[43] Both anions (Cl^- and Br^-) have their peaks located in the polar region at the right side of the graph, which is the hydrogen bond acceptor zone. This indicates that both are electronegative, and they can interact with the hydrogen bond donor. Therefore, they have a high affinity to accept hydrogen from the water molecules. Generally, an anion that has its peak further to the right side of the sigma profile graph is the most effective gas hydrate inhibitor because of its high electronegativity, which results in higher interaction with the water molecules. Hence, the Cl^- ion, which has its peak further to the right side, has a higher affinity with water as compared to the Br^- ion and therefore serves as a better hydrate inhibitor.

Cation Effect. Both cations (TMA and TPA) have their peaks located in the nonpolar region and thus have low affinity with water molecules. The reason for this is that water molecules have their peaks only in the polar regions, and they do not interact well with ions that have their peaks in the nonpolar region. This means that cations contribute very slightly to the process of hydrate inhibition. However, if the cations are compared between themselves, the TMA cation performs better than TPA because its highest peak is nearer to the polar region and thus has a better affinity with water molecules. TMA has a shorter alkyl chain length than TPA and hence can more effectively interact with water molecules as it is less bulky.[44]

Hydrogen Bond Donor Part. Figure 12 shows the sigma profile graph of ethylene glycol, glycerol, and water molecules. Both ethylene glycol and glycerol are standard HBDs, and they should have strong peaks in the HBD region. Generally, a substance that has marked peaks in either the HBD or HBA zone has a strong interaction with water. Both HBDs (ethylene glycol and glycerol) have shown similar affinities; however, glycerol shows a slightly lower peak difference with a water molecule, and hence it has a better hydrogen bonding donor affinity than ethylene glycol. The superiority of glycerol over ethylene glycol is based on the presence of three hydroxyl (OH) groups in glycerol as compared to two in ethylene glycol. Increasing the number of hydroxyl groups on a molecule generally enhances its ability to inhibit gas hydrate formation. This is because hydroxyl groups can form hydrogen bonds with water molecules in the hydrate structure, disrupting the lattice, thereby hindering hydrate formation.

From the sigma profile analysis, it is inferred that the DES with the Cl^- anion, TMA cation, and glycerol HBD is the best hydrate inhibitor, whereas the DES with the Br^- anion, TPA cation, and ethylene glycol HBD is the worst inhibitor. This is consistent with the results obtained experimentally.

Hydrogen Bonding Energies. The effectiveness of DESs as thermodynamic hydrate inhibitors can be determined through the comparison of hydrogen bonding strength.[23] The hydrogen bonding energies (E_{HB}) of all studies DESs were calculated using CASTEP and were corrected to account for basis set superposition errors (BSSE) with the counterpoise (CP) method. The obtained results are presented in Table 12 and plotted against average suppression temperatures from this study in Figure 13. It is evident from this graph that the temperature suppression value of the DES–hydrate system is directly proportional to the hydrogen bonding energy value for both 2 and 4 wt % concentrations. However, the linearity of

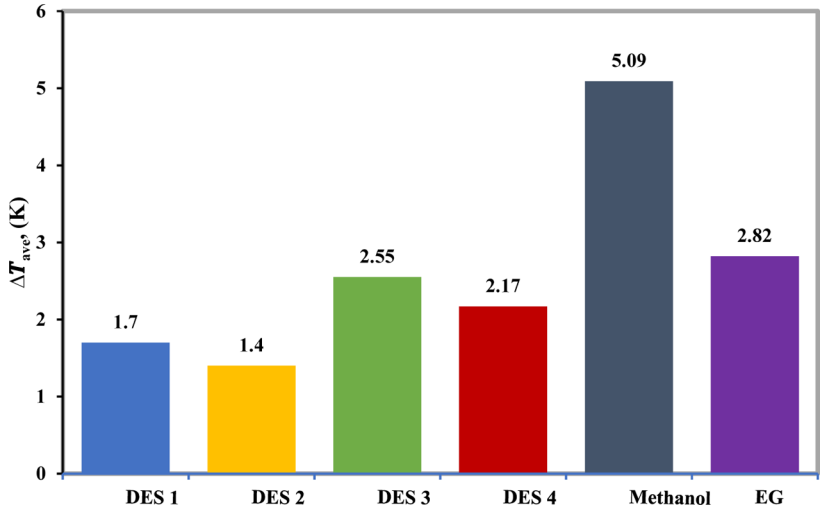

Figure 10. Comparison of the inhibition effects of the studied DESs on CH_4-CO_2 hydrates with commercial THIs, methanol, and ethylene glycol (obtained from literature[42]). The mass and molar concentrations of inhibitors are DES 1–4 wt % (0.68 mol %), DES 2–4 wt % (0.97 mol %), DES 3–4 wt % (0.78 mol %), DES 4–4 wt % (1.07 mol %), methanol–10 wt % (5.88 mol %), and ethylene glycol–10 wt % (3.12 mol %).

https://doi.org/10.1021/acs.jced.5c00067
J. Chem. Eng. Data 2025, 70, 3675–3689

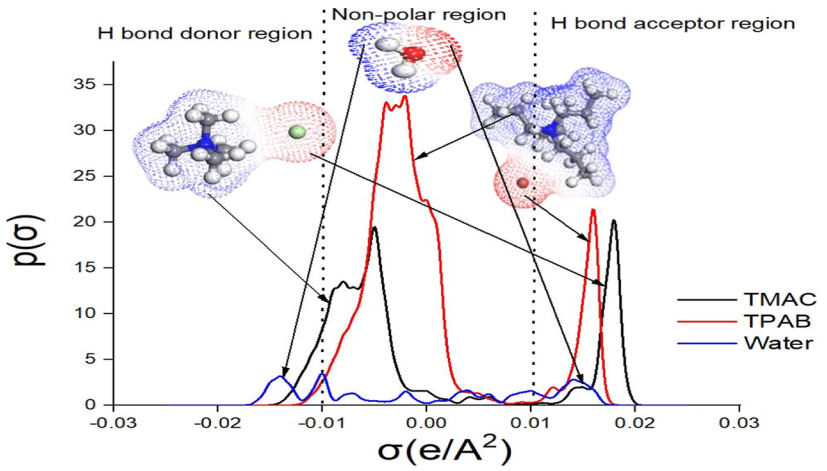

Figure 11. Sigma profiles (σ) of water and hydrogen bond acceptor (HBA) part of the DESs.

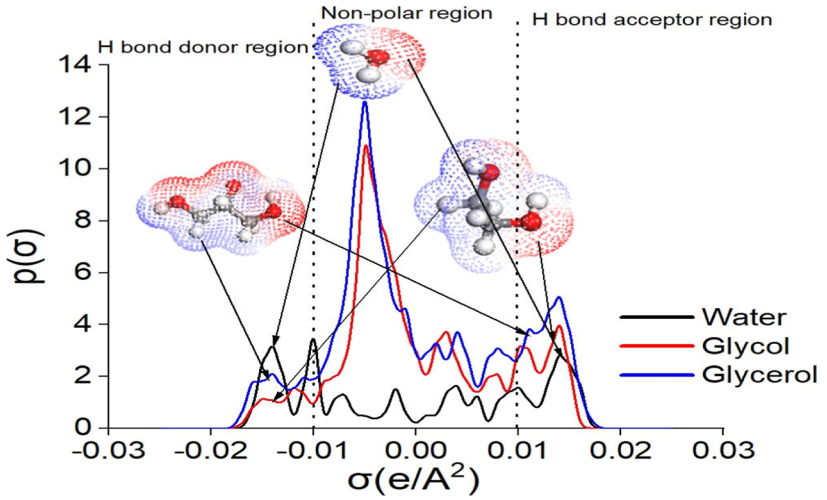

Figure 12. Sigma profiles (σ) of water and hydrogen bond donor (HBD) part of the DESs.

Table 12. Hydrogen Bonding Energy (E_{HB}) Values Calculated Using Super-Molecular Approach

DES	E_{HB} (kJ/mol)	ΔT_{ave} (K)	
		2 wt %	4 wt %
DES 3	−10.83	1.35	2.55
DES 4	−7.55	1.26	2.17
DES 1	−5.16	0.91	1.70
DES 2	−4.71	0.26	1.40

the relationship decreases with the concentration of DES in the aqueous solution. As shown in the graph, the R^2 value decreased significantly from 0.9386 to 0.6514 for 4 and 2 wt % solutions, respectively. The ranking of hydrogen bonding energies from the highest to the lowest is as follows: DES 3 (TMAC: glycerol) > DES 4 (TMAC: ethylene glycol) > DES 1 (TPAB: glycerol) > DES 2 (TPAB: ethylene glycol). The same ranking occurred with the experimental results, where DES 3 had the highest average suppression temperature and DES 2 had the lowest suppression. This ranking could be explained by the fact that between the two anions involved, Cl− anion has a higher polarized charge and thus shows a higher hydrogen bonding strength than Br− anion. From the hydrogen bonding energy analysis, it was deduced that the DES with the highest absolute value of hydrogen bonding energy is the best hydrate inhibitor.

COSMO-RS Sigma Profiles and Hydrogen Bonding Energies as Screening Tools. The validation section of this study confirms that the sigma profile and hydrogen bonding energies of DESs strongly correlate with their effectiveness as thermodynamic gas hydrate inhibitors. Consequently, this section presents a predictive analysis of four ammonium-based DESs, utilizing COSMO-RS sigma profiles and hydrogen bonding energies as screening tools to assess their gas hydrate inhibition potential (refer to Table 13).

SIGMA PROFILE

Hydrogen Bond Acceptor Part. *Anion Effect.* Figure 14 shows the sigma profile graph of TMAOH, TEAC, and water molecules. It is observed that anions (OH^- and Cl^-) have their peaks on the right side of the graph, which indicates their HBA ability. Therefore, they have a high affinity to interact with the water molecules. However, the OH^- ion has its peak further to the right side as compared to the Cl^- ion and hence it has a higher affinity with water molecules, which makes it a better gas hydrate inhibitor.

Cation Effect. It is observed that both cations (TMA and TEA) have their peaks positioned in the nonpolar region and thus have low affinity with water molecules. This means that

https://doi.org/10.1021/acs.jced.5c00067
J. Chem. Eng. Data 2025, 70, 3675−3689

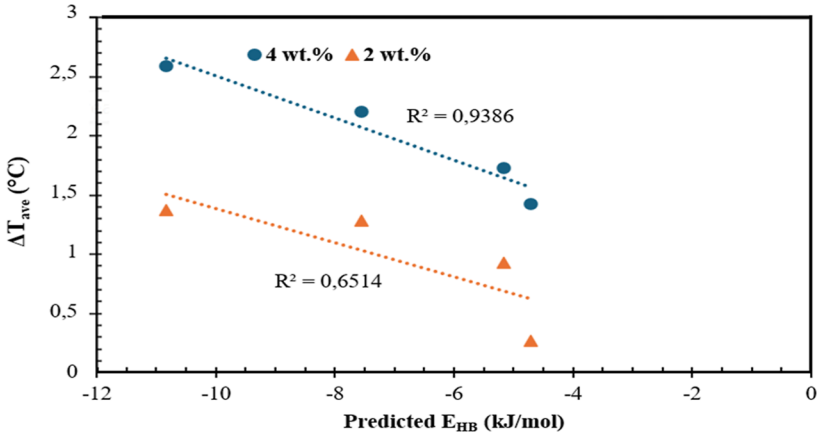

Figure 13. Average suppression temperature against predicted hydrogen bonding energy for 2 and 4 wt % aqueous solutions.

Table 13. List of Ammonium-Based DESs Used for Prediction

molar ratio	abbreviation
tetramethylammonium hydroxide (TMAOH) + glycerol (1:3)	DES 5
tetramethylammonium hydroxide (TMAOH) + urea (1:3)	DES 6
tetraethylammonium chloride (TEAC) + glycerol (1:3)	DES 7
tetraethylammonium chloride (TEAC) + urea (1:3)	DES 8

their contribution to gas hydrate inhibition is nominal. However, TMA has a better affinity with water than TEA because of its shorter alkyl chain length and the location of its highest peak closer to the HBD zone.

Hydrogen Bond Donor Part. Figure 15 shows the sigma profile graph of glycerol, urea, and water molecules. Both glycerol and urea are standard HBDs, and they should have strong peaks in the HBD region. It is observed from the graph that water has marked peaks in both HBD and HBA polar regions because of the presence of lone pairs of oxygen in its structure in addition to two hydrogen atoms. It also observed from the sigma profile graph that glycerol and urea have similar affinities with water molecules. However, glycerol has a slightly better HBD affinity than urea because of its marginally lower peak difference with a water molecule.

From the sigma profile analysis, it is deduced that the DES with the OH^- anion, TMA cation, and glycerol HBD is the best hydrate inhibitor, whereas the DES with the Cl^- anion, TEA cation, and urea HBD is the worst inhibitor. However, it is still necessary to justify this using the experimental data.

Hydrogen Bonding Energies. Table 14 shows the predicted hydrogen bonding energies of all DESs that were studied in the absence of experimental data.

It is observed from the table that the ranking of hydrogen bonding energies from the highest to the lowest is as follows: DES 5 (TMAOH/glycerol) > DES 7 (TEAC/glycerol) > DES 6 (TMAOH/urea) > DES 8 (TEAC/urea). This is consistent with the results obtained from the sigma profile analysis; however, experimental data are still necessary to justify the application of this computational approach.

CONCLUSIONS

In this work, the thermodynamic inhibition behavior of binary mixed hydrate systems (50−50 mol % CO_2 + CH_4) in the presence of the studied DESs is reported via experimental and computational approaches. It has been observed that all the investigated DESs considerably shifted the hydrate phase boundary to higher pressure and lower temperature regions. This shift increased with the increase in the concentration of DES in the aqueous solution from 2 wt % to 4 wt %. Among the experimentally considered DESs, DES 3 (tetramethylammonium chloride: glycerol) had the best gas hydrate inhibition ability with the average suppression temperature values of 1.35

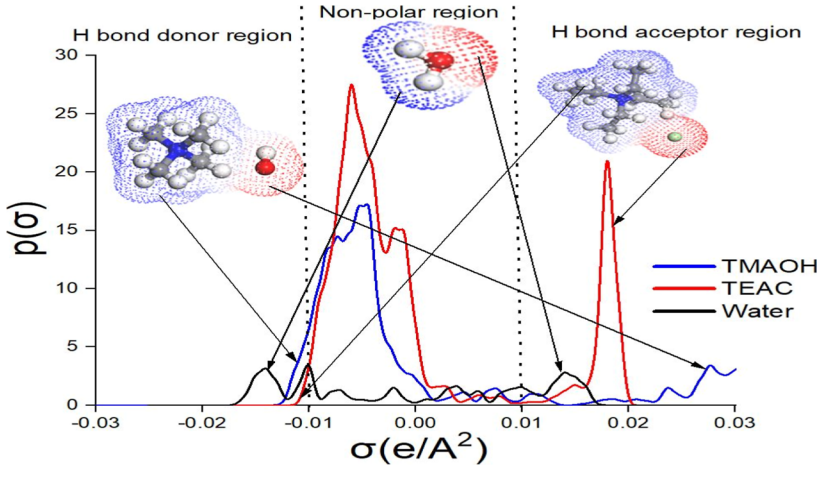

Figure 14. Sigma profiles (σ) of water and hydrogen bond acceptor (HBA) part of the DESs.

https://doi.org/10.1021/acs.jced.5c00067
J. Chem. Eng. Data 2025, 70, 3675−3689

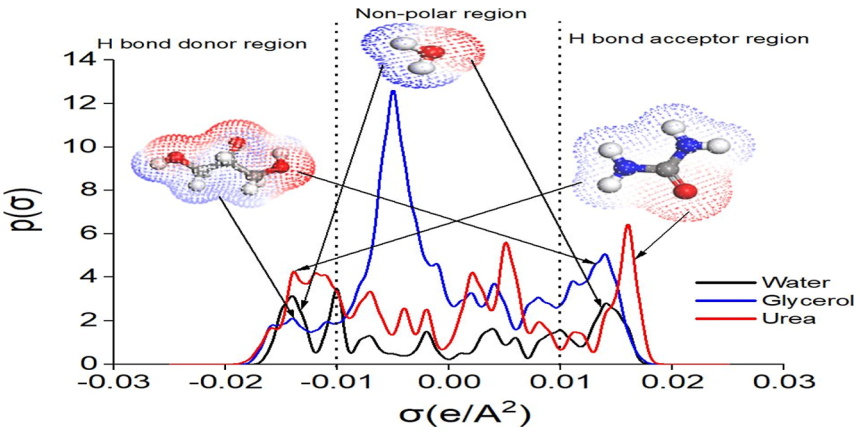

Figure 15. Sigma profiles (σ) of water and hydrogen bond donor (HBD) part of the DESs.

Table 14. Hydrogen Bonding Energy (E_{HB}) Values Predicted in the Absence of Experimental Data

DESs	E_{HB} (kJ/mol)
DES 5	−10.71
DES 6	−8.58
DES 7	−9.61
DES 8	−5.30

and 2.55 K at 2 and 4 wt % concentrations, respectively. The lowest inhibition ability was observed for DES 2 (tetra propylammonium bromide: ethylene glycol) with the average suppression temperature values of 0.26 and 1.40 K at 2 and 4 wt % concentrations, respectively.

This observation was validated using a computational approach through the analysis of sigma profile data and hydrogen bonding energy values obtained for the investigated DESs. It is apparent from the results obtained that the thermodynamic inhibition ability of DESs is profoundly dependent on the location of the anion, cation, and the hydrogen bond donor parts of DES in the interaction regions of the sigma profile. It appears that the DES with the highly electronegative anion and the highly electropositive hydrogen bond donor has a high thermodynamic inhibition ability. It is also observed that shorter alkyl chain length of the cation part of DES offers enhanced inhibition ability. The hydrogen bonding energies that were obtained in this study correlated well with the effectiveness of DESs as thermodynamic gas hydrate inhibitors. This high correlation between the predicted hydrogen bonding energies and the average suppression temperatures displayed the reliability of the computational approach used. It was deduced that the DES with the highest hydrogen bonding energy absolute value is the best hydrate inhibitor. The validated computational approach was successfully used as the prescreening tool to predict the inhibition ability of theoretically formulated DESs in the absence of experimental data. However, it is still critical that more experimental data should be collected as part of future research to justify its meaningful application in prescreening potential combinations of DESs for their possible application as THIs. The results obtained from this study proved that DESs have the potential to be promising alternatives to the currently used commercial THIs.

AUTHOR INFORMATION

Corresponding Author

Njabulo Mziwandile Zulu − *School of Chemical and Metallurgical Engineering, Oil and Gas Production and Processing Research Unit, University of the Witwatersrand, Johannesburg 2001, South Africa; Department of Chemical Engineering, Thermodynamics, Materials and Separations Research Group (TMSRG), Mangosuthu University of Technology, Durban 4031, South Africa;* orcid.org/0009-0005-5538-697X; Email: zulunm@mut.ac.za

Authors

Hamed Hashemi − *School of Chemical and Metallurgical Engineering, Oil and Gas Production and Processing Research Unit, University of the Witwatersrand, Johannesburg 2001, South Africa*

Kaniki Tumba − *Department of Chemical and Mineral Engineering, Faculty of Engineering, North-West University, Potchefstroom 2351, South Africa;* orcid.org/0000-0003-2685-3741

Victoria T. Adeleke − *Department of Chemical Engineering, Thermodynamics, Materials and Separations Research Group (TMSRG), Mangosuthu University of Technology, Durban 4031, South Africa*

Complete contact information is available at: https://pubs.acs.org/10.1021/acs.jced.5c00067

Author Contributions

The manuscript was written through the contributions of all authors. **Njabulo Mziwandile Zulu**: Conceptualization, methodology, investigation, writing—original draft, review, and editing. **Hamed Hashemi**: Supervision and contribution to the review and editing of the original draft. **Kaniki Tumba**: Supervision, project administration, funding acquisition, and review and editing of the original draft. **Victoria T. Adeleke:** Resource provision, simulation, and review and editing of the original draft.

Notes

The authors declare no competing financial interest.

ACKNOWLEDGMENTS

This study has been supported by the Mangosuthu University of Technology (MUT) and Witwatersrand University. The Mangosuthu University of Technology is appreciated for the financial support while undertaking this research project. The

authors would like to respectively appreciate S.S. Dladla and Dr N. Nkosi for their assistance with experimental data acquisition and graphical presentation.

REFERENCES

(1) Sloan, E. D.; Koh, C. A. *Clathrate Hydrates of Natural Gases*; 3rd Ed.; CRC Press, Taylor & Francis Group: Boca Raton, FL, 2008.
(2) Elhenawy, S.; Khraisheh, M.; Almomani, F.; Al-Ghouti, M. A.; Hassan, M. K.; Al-Muhtaseb, A. Towards Gas Hydrate-Free Pipelines: A Comprehensive Review of Gas Hydrate Inhibition Techniques. *Energies* **2022**, *15* (22), 8551−44.
(3) Patel, Z. D.; Russum, J. Flow Assurance: Chemical Inhibition of Gas Hydrates in Deepwater Production Systems. *Offshore* **2010**, *70* (6), 70−73.
(4) Cha, M.; Shin, K.; Kim, J.; Chang, D.; Seo, Y.; Lee, H.; Kang, S. P. Thermodynamic and Kinetic Hydrate Inhibition Performance of Aqueous Ethylene Glycol Solutions for Natural Gas. *Chem. Eng. Sci.* **2013**, *99*, 184−190.
(5) Kanda, H.; Uchida, K.; Nakamura, K.; Suzuki, T. Economics and Energy Requirements on Natural Gas Ocean Transportation in Form of Natural Gas Hydrate (NGH) Pellets. In *Proceedings of Fifth International Conference on Gas Hydrate*, 2005, pp 1275−1282.
(6) Tumba, K.; Reddy, P.; Naidoo, P.; Ramjugernath, D.; Eslamimanesh, A.; Mohammadi, A. H.; Richon, D. Phase Equilibria of Methane and Carbon Dioxide Clathrate Hydrates in the Presence of Aqueous Solutions of Tributylmethylphosphonium Methylsulfate Ionic Liquid. *J. Chem. Eng. Data* **2011**, *56* (9), 3620−3629.
(7) Brustad, S.; Løken, K.-P.; Waalmann, J. G. Hydrate Prevention Using MEG Instead of MeOH: Impact of Experience from Major Norwegian Developments on Technology Selection for Injection and Recovery of MEG. In *Offshore Technology Conference; Offshore Technology Conference*, 2005..
(8) Xiao, C.; Adidharma, H. Dual Function Inhibitors for Methane Hydrate. *Chem. Eng. Sci.* **2009**, *64* (7), 1522−1527.
(9) Kudłak, B.; Owczarek, K.; Namieśnik, J. Selected Issues Related to the Toxicity of Ionic Liquids and Deep Eutectic Solvents—a Review. *Environ. Sci. Pollut. Res.* **2015**, *22* (16), 11975−11992.
(10) Sivabalan, V.; Sahith, J. K.; Lal, B. Deep Eutectic Solvents as the New Norm for Oil and Gas Industry: A Mini Review. In *Proceedings of the Third International Conference on Separation Technology 2020 (ICoST 2020)*; Atlantis Press: Paris, France, 2020..
(11) Ghaedi, H.; Ayoub, M.; Sufian, S.; Lal, B.; Shariff, A. M. Measurement and Correlation of Physicochemical Properties of Phosphonium-Based Deep Eutectic Solvents at Several Temperatures (293.15 K−343.15 K) for CO 2 Capture. *J. Chem. Thermodyn.* **2017**, *113*, 41−51.
(12) Ghaedi, H.; Ayoub, M.; Sufian, S.; Shariff, A. M.; Lal, B.; Wilfred, C. D. Density and Refractive Index Measurements of Transition-Temperature Mixture (Deep Eutectic Analogues) Based on Potassium Carbonate with Dual Hydrogen Bond Donors for CO2 Capture. *J. Chem. Thermodyn.* **2018**, *118*, 147−158.
(13) de Andrade, D. C.; Monteiro, S. A.; Merib, J. A Review on Recent Applications of Deep Eutectic Solvents in Microextraction Techniques for the Analysis of Biological Matrices. *Adv. Sample Prep.* **2022**, *1*, 100007.
(14) Ijardar, S. P.; Singh, V.; Gardas, R. L. Revisiting the Physicochemical Properties and Applications of Deep Eutectic Solvents. *Molecules* **2022**, *27* (4), 1368.
(15) Jia, H.; Huang, P.; Wang, Q.; Han, Y.; Wang, S.; Zhang, F.; Pan, W.; Lv, K. Investigation of Inhibition Mechanism of Three Deep Eutectic Solvents as Potential Shale Inhibitors in Water-Based Drilling Fluids. *Fuel* **2019**, *244*, 403−411.
(16) Lee, D.; Go, W.; Oh, J.; Lee, J.; Jo, I.; Kim, K.-S.; Seo, Y. Thermodynamic Inhibition Effects of an Ionic Liquid (Choline Chloride), a Naturally Derived Substance (Urea), and Their Mixture (Deep Eutectic Solvent) on CH4 Hydrates. *Chem. Eng. J.* **2020**, *399*, 125830.
(17) Sivabalan, V.; Hasnor, N.; Lal, B.; Kassim, Z.; Shah Maulud, A. Tetraethylammonium Acetate and Tetraethylammonium Bromide-Based Deep Eutectic Solvents as Thermodynamic CO2 Gas Hydrate Inhibitors. *Appl. Sci.* **2020**, *10* (19), 6794.
(18) Khoo, Y. Z.; Ho, Y.-H.; Chang, K.-Y.; Chen, Y.-P.; Chen, L.-J. Dual Inhibition Effect of Reline Deep Eutectic Solvent on Methane Hydrate Nucleation and Formation. *Fuel* **2022**, *328*, 125376.
(19) Rasool, M. H.; Zamir, A.; Elraies, K. A.; Ahmad, M.; Ayoub, M.; Abbas, M. A. A Deep Eutectic Solvent Based Novel Drilling Mud with Modified Rheology for Hydrates Inhibition in Deep Water Drilling. *J. Pet. Sci. Eng.* **2022**, *211*, 110151.
(20) Klamt, A. Conductor-like Screening Model for Real Solvents: A New Approach to the Quantitative Calculation of Solvation Phenomena. *J. Phys. Chem.* **1995**, *99* (7), 2224−2235.
(21) Klamt, A.; Eckert, F. COSMO-RS: A Novel and Efficient Method for the a Priori Prediction of Thermophysical Data of Liquids. *Fluid Phase Equilib.* **2000**, *172* (1), 43−72.
(22) Khan, M. S.; Liew, C. S.; Kurnia, K. A.; Cornelius, B.; Lal, B. Application of COSMO-RS in Investigating Ionic Liquid as Thermodynamic Hydrate Inhibitor for Methane Hydrate. *Procedia Eng.* **2016**, *148*, 862−869.
(23) Saad Khan, M.; Lal, B. Pre-Screening of Ionic Liquids as Gas Hydrate Inhibitor via Application of COSMO-RS for Methane Hydrate. In *Solvents, Ionic Liquids and Solvent Effects*; IntechOpen, 2020; ..
(24) Gordon, M. S.; Jensen, J. H. Understanding the Hydrogen Bond Using Quantum Chemistry. *Acc. Chem. Res.* **1996**, *29* (11), 536−543.
(25) Abbott, A. P.; Capper, G.; Davies, D. L.; Rasheed, R. K.; Tambyrajah, V. Novel Solvent Properties of Choline Chloride/Urea Mixtures. *Chem. Commun.* **2003**, No. 1, 70−71.
(26) Smith, E. L.; Abbott, A. P.; Ryder, K. S. Deep Eutectic Solvents (DESs) and Their Applications. *Chem. Rev.* **2014**, *114* (21), 11060−11082.
(27) Verevkin, S. P.; Sazonova, A. Y.; Frolkova, A. K.; Zaitsau, D. H.; Prikhodko, I. V.; Held, C. Separation Performance of BioRenewable Deep Eutectic Solvents. *Ind. Eng. Chem. Res.* **2015**, *54* (13), 3498−3504.
(28) Nkosi, N.; Tumba, K.; Ramsuroop, S. Measurements of Activity Coefficient at Infinite Dilution for Organic Solutes in Tetramethylammonium Chloride + Ethylene Glycol Deep Eutectic Solvent Using Gas-Liquid Chromatography. *Fluid Phase Equilib.* **2018**, *462*, 31−37.
(29) Nkosi, N.; Tumba, K.; Ramsuroop, S. Tetramethylammonium Chloride + Glycerol Deep Eutectic Solvent as Separation Agent for Organic Liquid Mixtures: Assessment from Experimental Limiting Activity Coefficients. *Fluid Phase Equilib.* **2018**, *473*, 98−105.
(30) Nkosi, N.; Tumba, K.; Ramsuroop, S. Activity Coefficients at Infinite Dilution of Various Organic Solutes in the Deep Eutectic Solvent (Tetramethylammonium Chloride + 1,6 Hexanediol in the 1:1 Molar Ratio). *South African J. Chem. Eng.* **2019**, *27*, 7−15.
(31) Mbatha, B. P.; Ngema, P. T.; Nkosi, N.; Ramsuroop, S. Infinite Dilution Activity Coefficient Measurements for 1-Methyl-4-(1-Methylethenyl)-Cyclohexene as a Green Solvent for Separation. *J. Chem. Eng. Data* **2022**, *67* (4), 966−974.
(32) Nkosi, N.; Nkazi, D.; Tumba, K. Experimental Hydrate Phase Equilibrium Data Relevant to Bitter Melon, Pineapple, and Grape Juice Concentration. *ACS Omega* **2022**, *7* (39), 34741−34751.
(33) Xiao, C.; Wibisono, N.; Adidharma, H. Dialkylimidazolium Halide Ionic Liquids as Dual Function Inhibitors for Methane Hydrate. *Chem. Eng. Sci.* **2010**, *65* (10), 3080−3087.
(34) Parr, R. G.; Yang, W. G. P..; Yang, W. *Density Functional Theory of Atoms and Molecules*, Oxford University Press and Clarendon Press, New York and Oxford. *Int. J. Quantum Chem.* 1989.
(35) Boys, S. F.; Bernardi, F. The Calculation of Small Molecular Interactions by the Differences of Separate Total Energies. Some Procedures with Reduced Errors. *Mol. Phys.* **1970**, *19* (4), 553−566.
(36) Carolina Gipiela Corrêa Dias, M.; Oliveira Farias, F.; Cazelato Gaioto, R.; Kaspchak, E.; Conceição da Costa, M.; Igarashi-Mafra, L.; Mafra, M. R. Thermophysical Characterization of Deep Eutectic

https://doi.org/10.1021/acs.jced.5c00067
J. Chem. Eng. Data 2025, 70, 3675−3689

Solvents Composed by D-Sorbitol, Xylitol or D(+)Xylose as Hydrogen Bond Donors. *J. Mol. Liq.* **2022**, *354*, 118801.
(37) Jibril, B.; Mjalli, F.; Naser, J.; Gano, Z. New Tetrapropylammonium Bromide-Based Deep Eutectic Solvents: Synthesis and Characterizations. *J. Mol. Liq.* **2014**, *199*, 462−469.
(38) Rosmi, S. N. A. B. *Synthesis and Characterization of Deep Eutectic Solvents (Dess)*; Universiti Teknologi Petronas, 2015.
(39) Mjalli, F. S.; Naser, J.; Jibril, B.; Al-Hatmi, S. S.; Gano, Z. S. Ionic Liquids Analogues Based on Potassium Carbonate. *Thermochim. Acta* **2014**, *575*, 135−143.
(40) Servio, P.; Lagers, F.; Peters, C.; Englezos, P. Gas Hydrate Phase Equilibrium in the System Methane−Carbon Dioxide−Neohexane and Water. *Fluid Phase Equilib.* **1999**, *158*−*160*, 795−800.
(41) Qasim, A.; Khan, M. S.; Lal, B.; Shariff, A. M. Phase Equilibrium Measurement and Modeling Approach to Quaternary Ammonium Salts with and without Monoethylene Glycol for Carbon Dioxide Hydrates. *J. Mol. Liq.* **2019**, *282*, 106−114.
(42) Moujdin, I. A.; Khan, M. S.; Lal, B.; Abulkhair, H. A.; Alsaiari, A. Dual-Functional Gas Hydrate Inhibition of Tetramethylammonium Chloride for Carbon Dioxide-Methane Mixed Gas Systems. *Fuel* **2021**, *305*, 121598.
(43) Kurnia, K. A.; Pinho, S. P.; Coutinho, J. A. P. Evaluation of the Conductor-like Screening Model for Real Solvents for the Prediction of the Water Activity Coefficient at Infinite Dilution in Ionic Liquids. *Ind. Eng. Chem. Res.* **2014**, *53* (31), 12466−12475.
(44) Keshavarz, L. J. J.; Eslamimanesh A, M. A. Experimental Measurement and Thermodynamic Modeling of Methane Hydrate Dissociation Conditions in the Presence of Aqueous Solution of Ionic Liquid. *Fluid Phase Equilib.* **2013**, *354* (02), 312−318.

https://doi.org/10.1021/acs.jced.5c00067
J. Chem. Eng. Data 2025, 70, 3675−3689